Electronic materials



Microstructure, chemical inhomogeneity, and electronic properties of tin-incorporated Ga₂O₃ compounds

C. V. Ramana^{1,2,*}, Debabrata Das^{1,2}, Guillermo Gutierrez^{1,2}, Felicia S. Manciu³, and V. Shutthanandan⁴

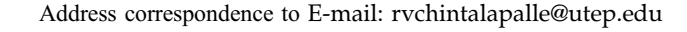
Received: 1 December 2021 Accepted: 7 April 2022 Published online: 16 June 2022

© The Author(s), under exclusive licence to Springer Science+Business Media, LLC, part of Springer Nature 2022

ABSTRACT

We report on the microstructure, dopant-induced changes in the chemical bonding, and electronic structure, chemical valence states of cations in Sn-incorporated gallium oxide (Ga₂O₃). Spectroscopic characterization of Sn-mixed Ga_2O_3 compounds $(Ga_{2-2x}Sn_xO_3, 0.00 \le x \le 0.3, Ga-Sn-O)$, which were produced by the high-temperature solid-state chemical reaction method, indicates that the Sn-mixing-induced changes in the microstructure and electronic structure are significant. X-ray photoelectron spectroscopic (XPS) analyses, which considered the Ga 2p doublet (Ga $2p_{3/2}$ and Ga $2p_{1/2}$ peaks), indicate that the Ga exists in its highest chemical valence state (Ga³⁺) in all of the samples, irrespective of Sn-content. The evolution of Sn peaks in XPS data indicates progressive increase in the Sn-content in Ga–Sn–O samples as x increases from 0.0 to 0.3. However, while no significant changes are seen in the Ga chemistry, formation of SnO₂ secondary phase was evident, especially with increasing Snconcentration. The XPS data confirm the Sn⁴⁺ chemical valence state of Sn-ions in all of the Ga–Sn–O samples. The energy-dispersive X-ray spectroscopic (EDS) mapping analyses reveal the localization of SnO₂ secondary phase in the parent matrix of Ga₂O₃. Combined EDS and XPS analyses indicate the secondary phase (SnO₂) formation becomes dominant for higher Sn-content. Corroborated with chemical analyses made by EDS and XPS, the Fourier infrared (FTIR) spectroscopic analyses also reveal the evolution of Sn-O bonds, which is reflected in the shift for the high-frequency stretching and bending of the GaO₄ tetrahedra, which structurally form the β -Ga₂O₃ phase. The detailed analysis of the FTIR data and peak evolution suggests a stronger interaction of Sn with Ga₂O₃ for

Handling Editor: Kevin Jones.





¹ Center for Advanced Materials Research (CMR), University of Texas at El Paso, 500 W University Ave, El Paso, TX 79968, USA

²Department of Mechanical Engineering, University of Texas at El Paso, 500 W University Ave, El Paso, TX 79968, USA

³Department of Physics, University of Texas at El Paso, 500 W University Ave., El Paso, TX 79968, USA

⁴Environmental Molecular Sciences Laboratory (EMSL), Pacific Northwest National Laboratory (PNNL), Richland, WA 99352, USA

 $x \ge 0.15$. A correlation between composition, crystal chemistry, and electronic properties is established in Ga–Sn–O compounds.

Introduction

Gallium oxide (Ga₂O₃), which is one among the wide band gap oxides, exhibits very interesting structural, physical, and chemical properties, which can be utilized in many of the current and emerging technological applications [1–15]. Ga₂O₃ and Ga₂O₃-based alloys can be readily integrated into numerous scientific and technological applications, which include electronics, optoelectronics, neuromorphic, energy storage and conversion, catalysis, and chemical sensors. The specific device application potential of these materials includes, but not limited to, the design and development of deep UV photodetectors, field-effect transistors (FETs), high power electronic devices, sensors, solar cells, transparent conducting oxides (TCOs), cost-effective light-emitting diodes (LEDs), contact, liquid eutectic and photocatalysts [6, 7, 10–14, 16–18].

The excellent thermodynamic stability coupled with ultra-wide band gap makes Ga₂O₃ attractive for solid-state power electronic and optoelectronic devices [1, 4, 5, 8, 9, 18, 19]. The bandgap of β -Ga₂O₃ is ~ 4.8 eV, which is second largest compared to the diamond, the well-known highest band gap material. Also, the band gap of Ga₂O₃ is considerably greater than other transparent conducting oxides (TCOs) such as In₂O₃, SnO₂ and ZnO. The recent massive attention and numerous studies performed on β -Ga₂O₃ indicate a possible future replacement of the well-established SiC and GaN power devices, which operate at extreme or ultra-high voltages [16–18]. On the other hand, Ga₂O₃ is also an interesting material from a fundamental science perspective; it exhibits six different polymorphs, namely the α , β , γ , δ , ε , and κ phases. However, compared to other polymorphs, the β-Ga₂O₃ polymorph (crystallizes in monoclinic crystal structure in the C^2/m space group) exhibits a very high and favorable chemical and thermal stability [19].

Recent attention and experimental and theoretical studies performed on β -Ga₂O₃ and β -Ga₂O₃-based alloys and composites resulted in some advancements in the field. Most importantly, several

researchers have directed their efforts to elucidating the effect of different metal ions into β -Ga₂O₃. Silicon doping into Ga₂O₃ effectively promotes the electrical conductivity since Si⁴⁺ acts as an electron donor and increases the free carrier concentration by a few orders of magnitude as compared to the undoped Ga_2O_3 [20–22]. Insight into the chemical formation energy and defect nature of transition metals doped into β -Ga₂O₃ was achieved by means of theoretical studies [23–25]. Using the DFT calculations, the shallow donor nature with a low formation energy was established for Nb-dopant as opposed to deep donor behavior of W, Mo, and Re as dopants into β - Ga_2O_3 [24]. The photocatalytic activity of doped β -Ga₂O₃ indicates that the specific ion and associated chemistry can influence the performance greatly [26-30]. Reasonably good number of studies were also performed on optical and optoelectronic properties. Complex photoluminescence (PL) properties were obtained by Eu-doping into colloidal γ-Ga₂O₃ nanocrystals which exhibit red and blue emission resulting from intra-4f orbital transitions. Dual bluegreen PL emission of Tb³⁺-doped Ga₂O₃ nanocrystals was also demonstrated [31]. The transition metal (TM) ion, such as Fe, Ti, and W, mixing or alloying into β-Ga₂O₃ indicated significant reduction and red shift in the optical band gap [13, 32-37]. However, the amount of red shift and spectral selectivity was found to be dependent on the specific TM-ion used for doping. Similarly, several existing works in the literature suggest that the overall chemistry, electronic structure, and optical properties can be tailored by considering the metal ions into β -Ga₂O₃ thin films or nanomaterials. The Cu-doped β -Ga₂O₃ thin films prepared by sputter deposition showed a marked decrease in the optical band gap [38]. The band gap reduction was attributed to the impurity energy levels formed by Cu-ions doped into β -Ga₂O₃ [38]. A red-shifted band gap was observed for W- and Tidoped β-Ga₂O₃ polycrystalline thin films produced using different thin-film deposition techniques [33, 39–41]. Thus, it is clear that the structural, chemical, and electronic properties of the resulting materials highly depend on the nature, chemistry,



valence state, and site occupation of the specific dopant ion into β-Ga₂O₃.

The present work deals with the Sn-incorporation induced effects on the microstructure, chemical bonding, and electronic properties of Ga₂O₃. The impetus to study the effect of Sn is derived from the following considerations. Similar to Ga₂O₃, SnO₂ is also an interesting semiconductor and has been explored for utilization in TCOs and sensors [42–49]. Therefore, we believe that understanding the science of Sn incorporation into Ga₂O₃ and understanding their properties are beneficial not only from a fundamental science perspective but also to derive new properties and phenomena, which can facilitate designing materials for advanced electronics and optoelectronics. In fact, Sn-doping into Ga₂O₃ has been considered widely in recent years [50-59]. The Sn-doped Ga₂O₃ single crystals were produced using the float zone method, where electrical resistivity and carrier concentration were shown to be tailored based on the amount of Sn doped into Ga₂O₃ [50]. Similarly, the viability of Sn-doped Ga₂O₃ as a GaN-based optical device for TCOs has also been explored [53]. The MOCVD-produced thin films of Sn-doped Ga₂O₃ exhibit n-type conductivity with a carrier concentration of 1.95×10^{17} cm⁻³ and a Hall mobility of 0.9 cm²Vs⁻¹ [56]. Similarly, it was found that the Sndoping into Ga₂O₃ improves the overall electrical conductivity and Hall mobility [58]. Most recently, Ryou et al. studied the structural, chemical, and photocatalytic properties of Sn-doped β-Ga₂O₃ nanomaterials synthesized by a facile hydrothermal chemical method [51]. It was found that the photocatalytic activity of the Sn-doped (0.7 at%) β-Ga₂O₃ nanostructures significantly enhanced compared to that of intrinsic β -Ga₂O₃. Based on the results, the authors suggest the possible new opportunities to design highly effective β-Ga₂O₃-based photocatalysts for applications in environmental remediation, disinfection, and selective organic transformation [51]. However, despite the fact that Sn doping of Ga₂O₃ single crystals and thin films has been explored quite extensively in recent years, the fundamental aspects of Sn mixing into Ga₂O₃ inorganic compounds have not been considered much in the literature. Such a deeper understanding of the crystal structure, electronic structure, and structure-property correlation is the key to manipulate the materials for desired applications. Therefore, in the present work, we employed spectroscopic methods, namely X-ray

photoelectron spectroscopy (XPS), energy-dispersive X-ray spectrometry (EDS), and Fourier transform infrared spectroscopy (FTIR), to probe the electronic structure and chemical inhomogeneity in addition to chemical bonding information on the Sn-mixed Ga₂O₃ compounds. As presented and discussed in this paper, such a comprehensive understanding of the microstructure details, chemical homogeneity, and associated effects on the electronic structure and properties as a function of Sn concentration enhances our ability to design the materials with controlled phase and properties for practical device applications.

Materials and methods

Synthesis

The tin (Sn)-mixed gallium oxide (Ga₂O₃) compounds were produced via the high-temperature, solid-state chemical reaction method [3]. In order to obtain the homogenous compounds in the series of Sn-mixed Ga₂O₃ (referred to as Ga-Sn-O), high-purity Ga₂O₃ (99.99%) and SnO₂ (99.99%) powders were mixed thoroughly. The ratio for Sn was adjusted based on a balanced stoichiometry following the chemical formula $Ga_{2-2x}Sn$ [60] ${}_{x}O_{3-\delta}$ (referred to as Ga–Sn–O), where x is the amount of Sn introduced. Compounds were prepared by varying the concentration of Sn in the range of x = 0.0-0.3. In the solidstate synthesis route adopted, we first initiated the process by grinding the powders using a mortar and pestle under a volatile liquid environment. This ensures homogeneous mixing and the formation of smaller size particles. The sequence of the steps and various stages involved in synthesis of Ga-Sn-O samples are schematically represented in Fig. 1.

The mixture was calcined at a temperature closer to the melting point of the material. In this case, the mixed compound was heat-treated at 1100 °C for 12 h in a muffle furnace. The ramp rate used for heating and cooling was 5 °C/min. After calcination of the sample, the mixture was ground again by introducing polyvinyl acetate (PVA). Under the presence of PVA, the mixture was ground into a fine powder, which was then used to make pellets. The pellets were made by pressing the final Ga–Sn–O powder at 1.5 tons for 1 min and had dimensions of 8 mm diameter and 2 mm thickness.



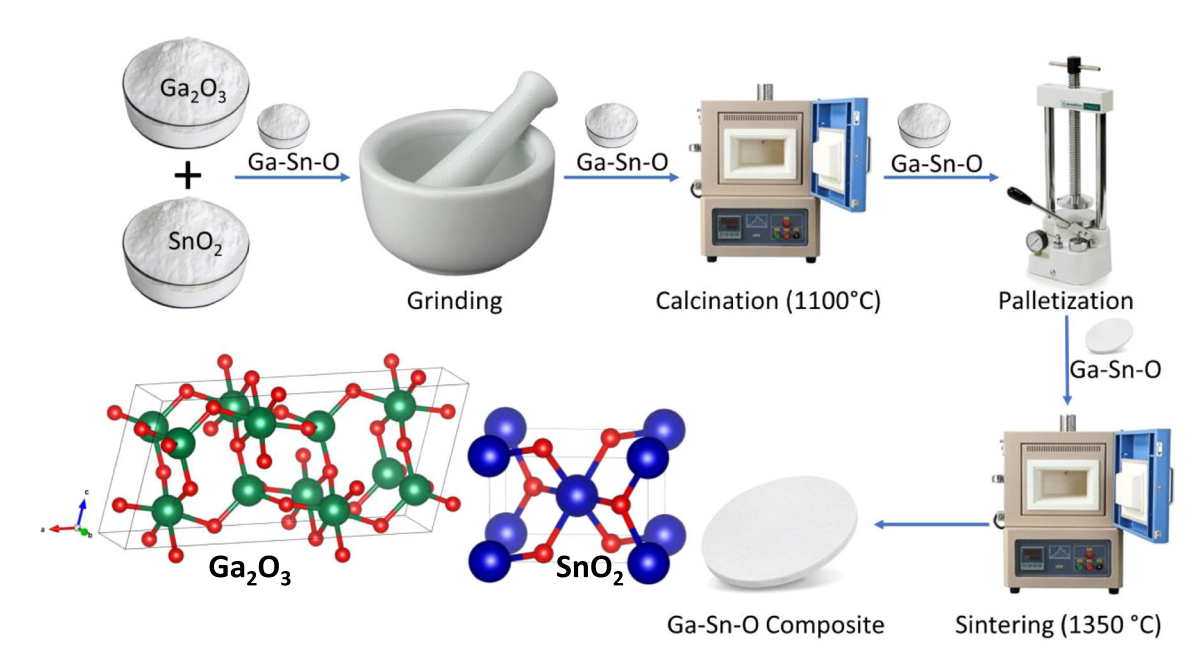


Figure 1 Schematic representation of the synthesis procedure employed for Ga-Sn-O samples. The sequence of the steps and various stages involved in synthesis of Ga-Sn-O samples are indicated.

The second stage of the Ga–Sn–O chemical compound synthesis involved a sintering process. The pellets were subjected to the second heat treatment, i.e., sintering, at higher temperatures. The objective was to obtain a relatively dense material by closing the pores of the powder particles and also to eliminate any other defects that may have been present. The sintering temperature, which is typically higher than the calcination temperature, was set to 1350 °C for 12 h while maintaining the same ramp rate as in the calcination. The final products, which are Ga–Sn–O materials with a variable Sn concentration (x), thus obtained were subjected to characterization to understand the structure, composition, and electrochemical properties.

Characterization

Scanning electron microscopy (SEM)

The Ga–Sn–O samples were used to study the morphological characteristics using the FEI Magellan 400 scanning electron microscope. The SEM provides sub-nanometer spatial resolution. The samples were gold-coated (< 5 nm thickness) before imaging to optimize the surface properties under SEM. The accelerating voltage was limited to 5 kV, and the working distance was kept below 4 mm.

Energy-dispersive x-ray spectroscopy (EDS)

To understand the phase separation and Sn-chemistry, we performed energy-dispersive X-ray spectroscopy (EDS) measurements on select compositions. For the purpose of EDS measurements, scanning electron microscopy (SEM, Hitachi High-Tech America, Inc, USA) was employed while measurements were performed using the backscattered electron mode. An elemental compositional analysis was performed using EDS with the use of x-ray color mapping to allow for the approximate determination of elements present and their distribution characteristics.

X-ray photoelectron spectroscopy (XPS)

XPS characterization of intrinsic and doped/alloyed Ga_2O_3 materials proved to be quite useful in our previous studies on understanding the effect of dopants on the electronic structure and properties [13, 32, 34, 35, 37, 61]. Therefore, we implemented the previously established procedures and methods to characterize the Ga–Sn–O compounds using XPS. For clarity purpose, the details of XPS measurements and analytical procedures performed are as follows. The XPS scans of Ga–Sn–O compounds were obtained employing Kratos Axis Ultra DLD spectrometer using Al K α monochromatic X-ray source



(1486.6 eV). The survey and high-resolution (HR) scans were carried out at a pass energy of 160 and 40 eV, respectively. Survey scans and high-resolution spectra of Ga 2p, Fe 2p, O 1 s, C 1 s and Ga 3d peak regions were obtained analyzed to understand the effect of Sn doping into Ga₂O₃. The survey and highresolution (HR) scans were carried out at a pass energy of 160 and 40 eV, respectively. Charge neutralizer was set to a value of 3.5 eV as these are insulating ceramic oxide samples. Raw XPS data were fitted with the help of CasaXPS software using Gaussian/Lorentzian (GL(30)) line shape and Shirley background correction. Survey scans were collected over the binding energy (B.E.) range of 1400–(–) 5 eV, whereas HR spectra of Ga 2p, Fe 2p, O 1 s, C 1 s, and Ga 3d peak regions were obtained with at least 8 number of sweeps for each of them depending on the clarity of the peaks. Though both the Ga peaks (i.e., Ga 2p and 3d) were collected for confirmation, only Ga 2p spectra are depicted in order to avoid confusion coming from the interference of Ga 3d peak with O 2 s peak as both the peaks are very closely situated. Detailed discussion on sample preparation techniques for XPS, precautions taken during sample transfer from the furnace atmosphere to the XPS analysis chamber and during XPS data collection, and particular instrumental parameters used for scanning can be found elsewhere. Specifically, these procedures adopted were found to be efficient to evaluate both intrinsic and doped Ga₂O₃ compounds. The binding energy of carbon (C 1 s) peak at 285 eV was used for charge referencing all other HR spectra. Estimation error of \pm 0.01 at.% was considered in order to obtain elemental concentration.

Fourier transform infrared (FTIR) spectroscopy

The Fourier transform infrared, FTIR, spectra analysis allows the vibration of atoms or groups of atoms to be observed; this will allow us to confirm the quality and bonding of the Ga–Sn–O composition with relation to the amount of Sn incorporated on the $Ga_{2-x}Sn_xO_3$ samples. The far-IR (150–400 cm⁻¹) and mid-IR (400–4000 cm⁻¹) transmission spectra were recorded with a vacuum-based Bruker IFS 66v system. For these analyses, the samples were prepared in the form of pellets by embedding them in a CsI matrix. Two different beam splitters, a Ge-coated mylar and a KBr, as well as two deuterated triglycine

sulfate (DTGS) detectors, were employed for such measurements. Each IR spectrum is the result of an accumulation of 256 scans at a resolution of 4 cm⁻¹.

Results and discussion

Microstructure and chemical inhomogeneity

The microstructure and chemical inhomogeneity of the Ga-Sn-O samples were first analyzed by the combined use of SEM and EDS mapping analyses. Then, the evolution of chemical composition, chemical valence states, chemical inhomogeneity, and influence of Sn incorporation on lattice vibration of the samples was further confirmed by means of XPS and FTIR studies. Additionally, we validated our findings with structural and optical analysis (XRD and UV-Vis spectroscopy). Figure 2 depicts topographical fingerprint of Ga-Sn-O compounds for x = 0.00-0.30. The overall morphology until x = 0.20showed least significant modulation with increasing Sn incorporation. Average particle size distribution along with topographical signature was almost invariant with lower Sn concentration. Higher Sn content (x = 0.3) showed drastic change in morphology of the samples. The grains were fractured and distorted throughout the surface. Also, average particle size reduced drastically. This anomalous behavior can be explained through gradual evolution of single-phase Ga-Sn-O versus multiphase Ga-Sn- $O + SnO_2$ composites with increasing concentration of Sn. Starting with pure Ga_2O_3 (Ga–Sn–O: x = 0.0), smaller amount of Sn incorporation settled in homogeneous composition of Ga-Sn-O throughout the matrix. As it crossed the solubility limit (we believe x = 0.15 in this case, confirmed through XRD analysis) of Sn into the host material, there was a tendency to form multiple phases and to introduce chemical inhomogeneity inside the complex composites. During the fabrication process of such high Sn concentrated Ga-Sn-O composites at elevated temperature, the SnO₂ binary phase might tried to segregate out of the host matrix. During the process of phase segregation, it formed distorted grains. To get an elaborative understanding about this chemical inhomogeneity and coexistence of multiphase complex composites, we performed the EDS analyses. The data of the EDS analyses are presented in Fig. 3.



Assertively, there is an evident signature in the SEM images for the formation of SnO₂ secondary phase with increasing Sn concentration. Dissociated SnO₂ crystals, which appeared as a secondary phase in XRD analyses reported elsewhere², are found to be accumulating throughout the surface of host β-Ga₂O₃ grains. A clear difference in contrast is reflected in SEM/EDS mapping images (Fig. 3a) providing evidence for such chemically induced surface segregation of Ga–Sn–O composites for x = 0.2. Small molelike features appear with Sn incorporation. Owing to the bigger crystal size of SnO₂, it is quite natural that the parasitic phase will try to come out of the host and try to accumulate along the circumference of the same. As we keep increasing the Sn-concentration, further phase separation occurs and small parasitic SnO₂ crystals start agglomerating to form bigger SnO₂ grains, which can be visually distinguished from Ga₂O₃ with the help of color contrast in the SEM images. Finally, for higher amount (x = 0.3) of Sn incorporation, duly sintered at optimized temperature, there was a prominent evidence of crack formation in the host Ga₂O₃ crystals (Fig. 3b), which was the result of rigorous phase separation between Ga₂O₃ and SnO₂.

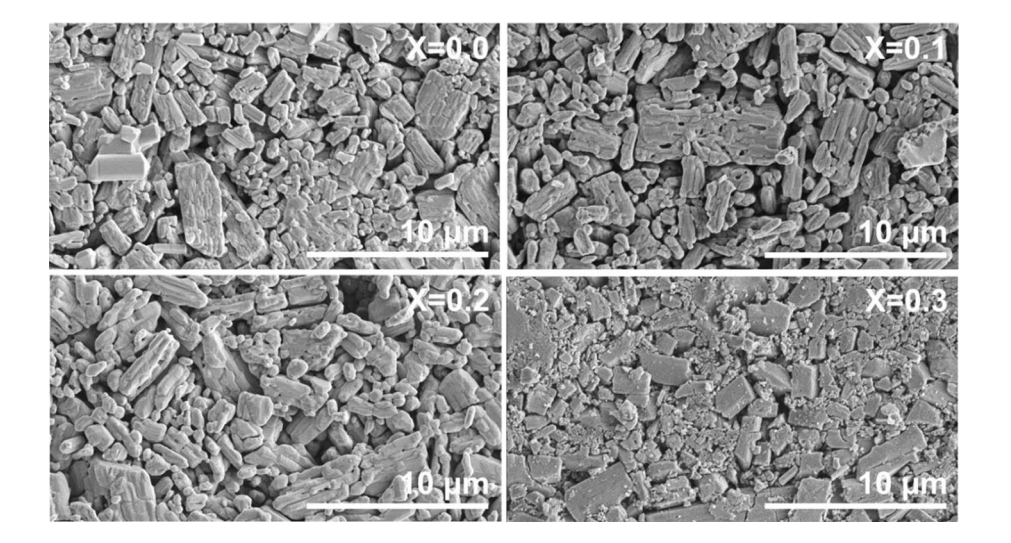
The XRD analyses coupled with refinement of the data also indicated that the increasing Sn concentration results in the formation of single phase Ga–Sn–O materials for lower Sn-content while composite formation occurs at higher Sn-concentration, where monoclinic β -Ga₂O₃ and tetragonal SnO₂ coexist. The XRD and refinement data and related analyses were reported previously². The results indicate that solubility limit of Sn intermixing appears to be x = 0.15, at

Figure 2 High-resolution SEM images of Ga–Sn–O composites for x = 0.0–0.3 showing gradual evolution of topographical signature and possible phase segregation along with distorted grain formation after a critical value of Sn incorporation.

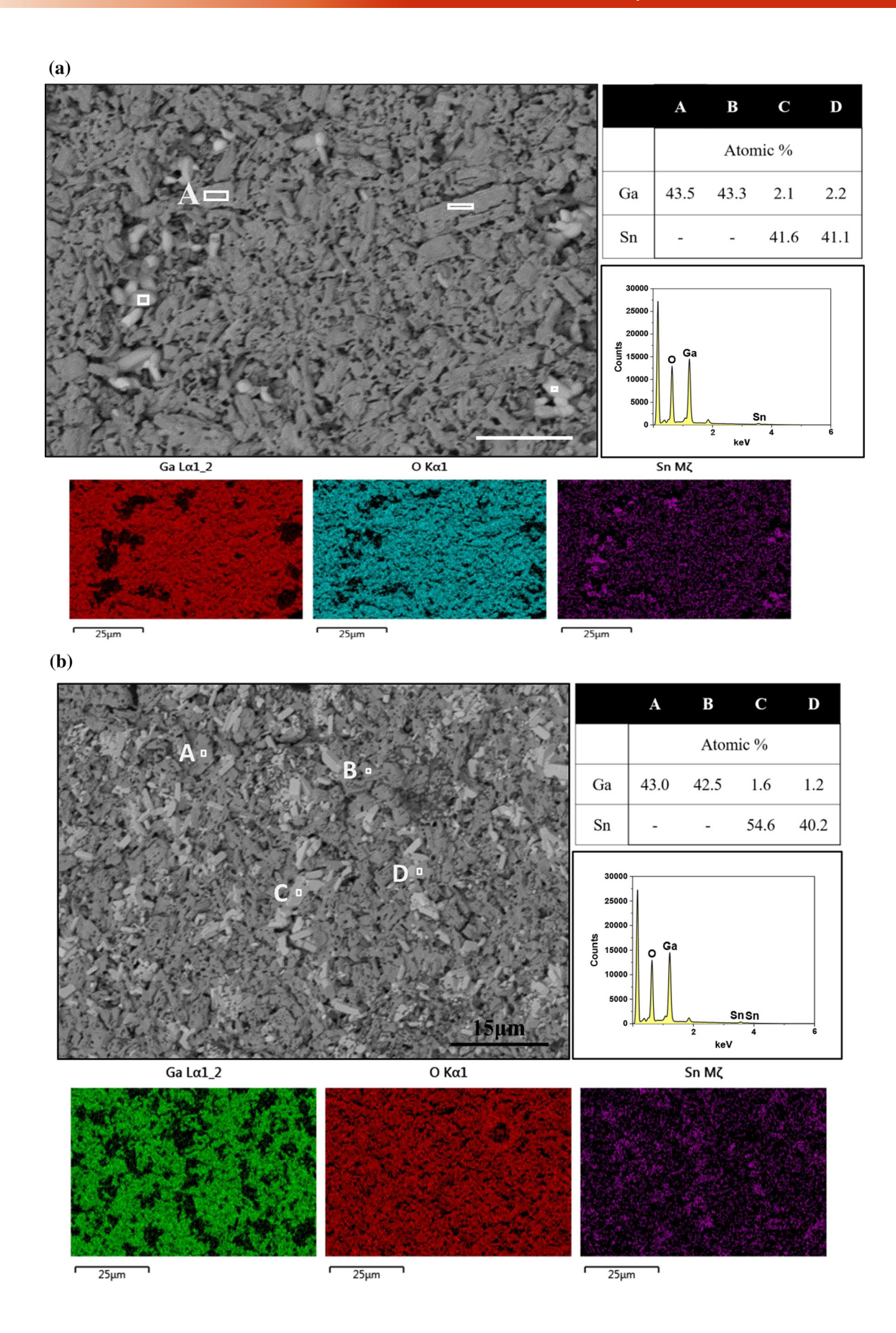
Figure 3 a EDS data of Ga-Sn-O compounds. SEM image of▶ Ga-Sn-O composition with x = 0.2 at 3000X in the backscattering electron mode (upper panel) shows the elemental contrast. The marked regions of A, B, C, and C indicate the representation of Ga-oxide and Sn-oxide areas. It can be noted (Table, upper panel) that the Sn isolates forming SnO₂ as a secondary phase. The EDS color mapping of Ga, Sn, and O elements (lower panel) indicates the composition distribution of the respective elements. **b** EDS data of Ga-Sn-O compounds. SEM image of Ga-Sn-O composition with x = 0.3 at 3000X in the backscattering electron mode (upper panel) shows the elemental contrast. The marked regions of A, B, C, and C indicate the representation of Ga-oxide and Sn-oxide areas. It can be noted (Table, upper panel) that the Sn isolates forming SnO₂ as a secondary phase. The EDS color mapping of Ga, Sn, and O elements (lower panel) indicate the composition distribution of the respective elements.

which point the formation of SnO_2 tetragonal phase formation inside monoclinic β - Ga_2O_3 host matrix was evident [3]. Quantitative analyses revealed that, for Sn in the composition, x = 0.15 results in the first appearance of the SnO_2 tetragonal phase as a secondary phase. The higher amount of SnO_2 phase formation occurs at x = 0.3, where the identified tetragonal SnO_2 phase was about $10-12\%^3$. We believe that, as noted in the EDS mapping analyses of the microstructure, the randomly oriented tetragonal structure SnO_2 coexists with monoclinic Ga_2O_3 at higher Sn-concentrations as evidenced in the structural characterization of the resulting of materials.

The overall particle size distribution was also tailored according to increasing Sn incorporation. Figure 4 shows the histogram of size distribution for









Ga–Sn–O composites for x = 0.00–0.30. Average particle size as a function of Sn concentration is shown in Fig. 4e. Starting with pure Ga₂O₃, where the average size was found to be \sim 770 nm, there was a drastic increment in average size distribution for x = 0.10, followed by gradual decreasing trend till x = 0.30. The data presented in both Figs. 2 and 4 confirmed better nucleation with bigger grain formation till the solubility limit of Sn in Ga₂O₃. Beyond that critical limit, the overall complex composite started decomposition into multiphase compound. Through this process of phase segregation from the host material, bigger particles/grains started breaking down into smaller form and showed in decreasing trend in nature. The phase separation and successive smaller particle formation were highest for x = 0.30.

The EDS results (Fig. 3) and analyses provided direct evidence for Sn-oxide secondary phase formation. In the EDS data of a representative sample (Fig. 3a), where x = 0.2, the first appearance of nucleation of SnO2 is seen, although not quite extensive. The Ga-Sn-O samples probed at various areas (spot analysis mode) to examine the composition distribution. As seen in the image, bright clusters of particles are visible throughout. These are believed to be SnO₂ particles. The areas marked A and B are proved to be Ga₂O₃ particles based on the ratio from the atomic percentage present. The areas marked C and D seem to be SnO2 based on the ratio of the atomic percentages. In the color maps, the areas where Sn is present are clearly visible and show gaps on the Ga map. The elemental contrast between the particles allows the ability to differentiate between different particles, where the Sn particles appear brighter. These areas are confirmed to be SnO₂ from spot analysis. The color mapping shows a clear difference in the area between the Ga enriched areas as compared to the Sn enriched areas.

The SEM and EDS data of Ga–Sn–O samples with highest doping level of Sn (x = 0.3) showed (Fig. 3b) interesting features. While the morphology is comparable to that of Ga–Sn–O samples with lower Sn content, the presence of a higher degree of Sn clusters can be noted. Also, the Sn clusters are dispersed throughout the sample surface. Two areas marked A and B are particles of Ga_2O_3 which is evident from the chemical information (atomic percentages). The brighter particles, which are marked C and D, are again assumed to be SnO_2 , which is further confirmed by the atomic percentage ratios obtained. The

formation of SnO_2 secondary was also evidenced in XRD studies. In the EDS color maps, there are relatively more areas/regions containing Sn visible. Further, these Sn-areas scattered relatively evenly throughout the samples. The map sum spectrum contains a higher amount of Sn present, indicating there are more SnO_2 particles produced throughout the matrix and Sn has segregated into its own separate phase of SnO_2 .

Chemical bonding—FTIR

Topographical energy-dispersive mapping in the previous section clearly demonstrates the gradual tailoring of the chemical composition with increasing incorporation of Sn into the Ga₂O₃ host matrix. To further understand and probe the chemical bonding evolution in Ga-Sn-O samples, we relied on FTIR spectroscopic analyses, particularly useful to address the evolution of lattice vibration as a function of Sn incorporation. The FTIR data of Ga-Sn-O samples are presented in Figs. 5 and 6. For comparison, the FTIR spectra of intrinsic Ga₂O₃ and SnO₂ are shown in Fig. 5. Depending on peaks in pure Ga₂O₃, we have identified 14 significant peaks, named alphabetically. The motivation is to understand tailoring of notable peaks in host Ga₂O₃ with increasing incorporation of Sn. Figure 6a and b shows the magnified FTIR spectra of Ga–Sn–O samples (x = 0.0–0.3) from 200 to 600 cm^{-1} and $600 \text{ to } 1000 \text{ cm}^{-1}$ spectral regions, respectively. All of the identified peaks for all concentrations of Sn are presented in Table 1. For mid-IR spectra, the characteristic bands of β-Ga₂O₃ appear at 456 [60, 62-64] and 620 [64-66] cm⁻¹ in undoped sample; therefore, peaks F and L were assigned as Ga₂O₃ related peaks. The region between 459 and 476 cm⁻¹ contains 3 associated Ga₂O₃ peaks (F, G and H). Peak F remained same for x = 0.05, but it was not present in FTIR spectra as the Sn-concentration increases in Ga-Sn-O samples. Near to peak H, there was a peak identified to be related to SnO₂ at 482 cm⁻¹. Therefore, shift of H peak with increasing Sn concentration suggested an interaction between the Ga and Sn atoms. Substitutional versus interstitial replacement of Ga atoms by Sn with increasing alloying composition can be evaluated with this peak tailoring. In the same area between 400 and 600 cm⁻¹, we noted a distinct feature at 527 cm⁻¹ which disappeared as the Sn concentration increased. Then, another peak at 594 cm⁻¹ appeared in sample with



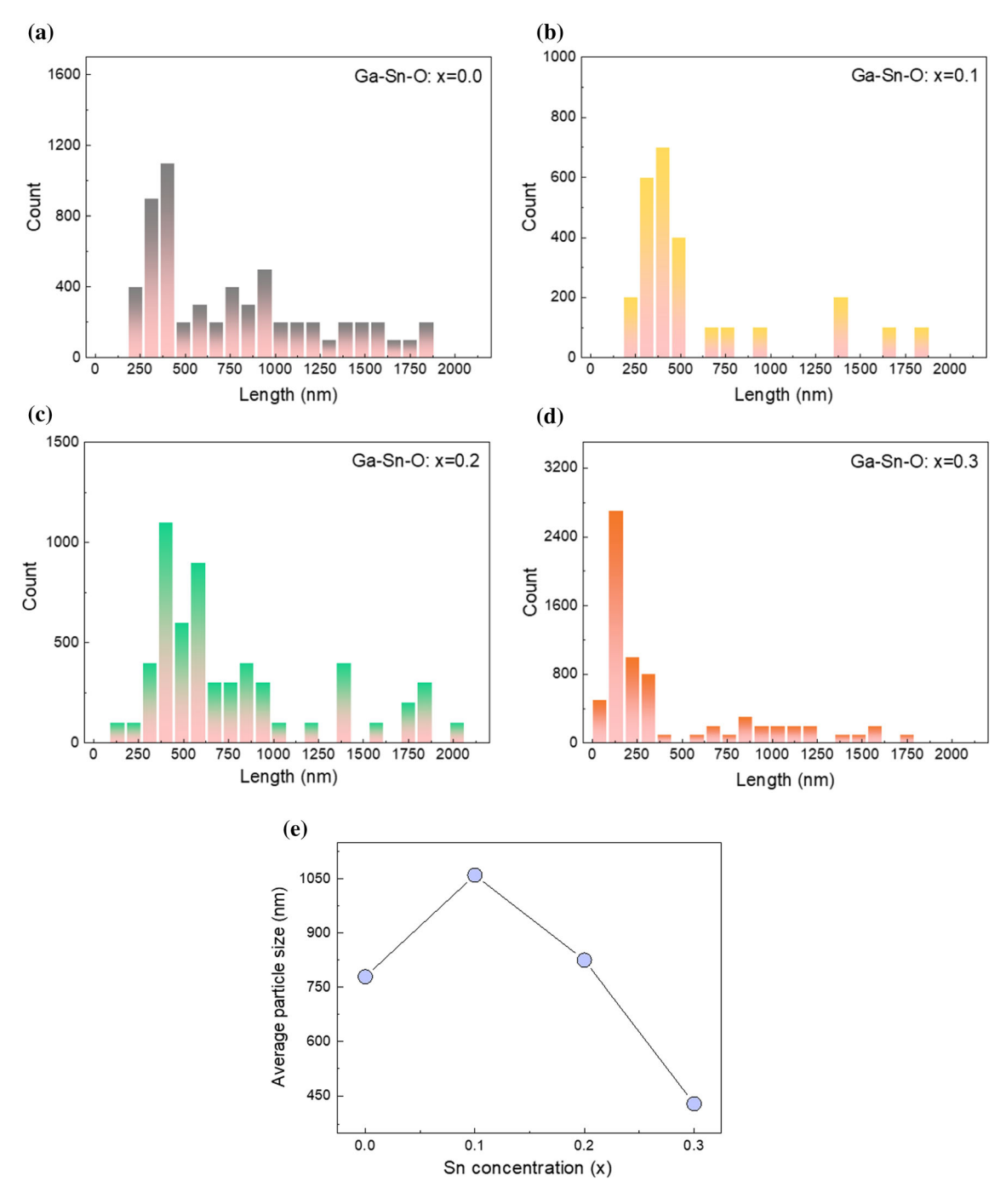


Figure 4 a–d Particle size distribution of Ga–Sn–O composite for x = 0.00–0.30. e Average size distribution for various Sn incorporation into Ga–Sn–O composite.

x = 0.3; this peak was in vicinity of a peak generally assigned to SnO₂ (614 cm⁻¹). It has been reported in the literature that Sn bonded to oxygen or hydroxyl groups may appear similarly as noted in this work. Song [67] attributed the weakening of this feature to the following reaction:

$$Sn-OH+HO-Sn\rightarrow Sn-O-Sn+H_2O$$

The band at 621 cm⁻¹, peak K, identified previously for β -Ga₂O₃ [67–70] began to shift to the right where a peak at 644 cm⁻¹ was identified on SnO₂ [8, 9, 11, 69, 71]. Another band at 690 cm⁻¹ had a



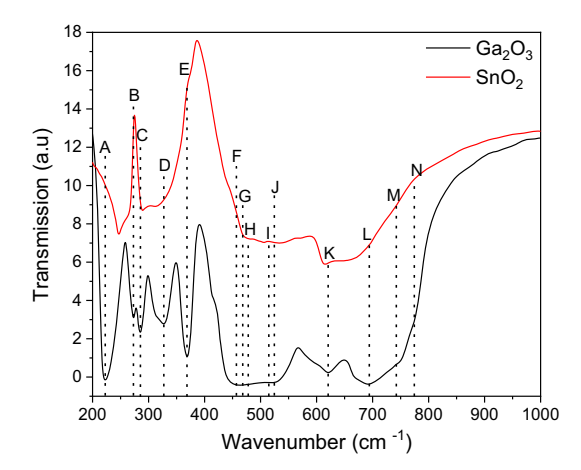
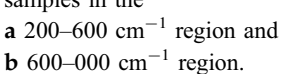


Figure 5 Transmission mode FTIR spectra of pure Ga₂O₃ and SnO_2 .

Other peaks found on the far-IR spectra were assigned to Ga₂O₃ and were found on all Ga-Sn-O samples independent of Sn concentration. Peak A and peak C widen and shift to the right as the Sn concentration increases. A SnO2 peak was identified at 246.8 cm⁻¹ and 289.3 cm⁻¹ suggesting a stronger interaction with Sn as concentration increased beyond x = 0.15. Peaks B and E shift with increased concentration, although an Sn interaction could not be confirmed. This might be due to tailoring of lattice vibration with substitutional Ga replacement by Sn atoms. Peak D has a variation in position that could not be confirmed as an effect of Sn addition even though a peak at 289.3 cm⁻¹ was identified for SnO₂ Figure 7 shows the FTIR peak shift with respect to

Figure 6 Transmission mode FTIR spectra of Ga-Sn-O samples in the



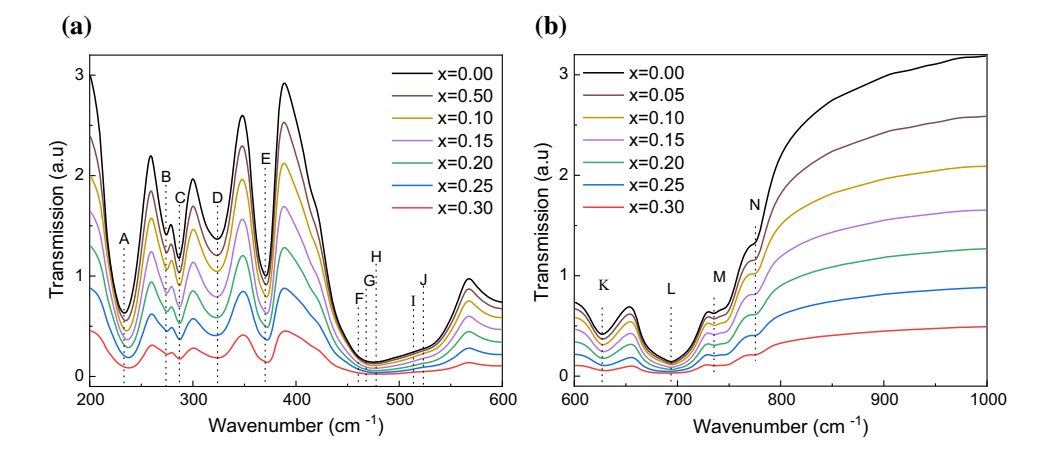


Table 1 Comparison of FTIR peak positions of undoped and Sn-incorporated Ga-Sn-O samples

Peak	Ga ₂ O ₃	x = 0.05	x = 0.10	x = 0.15	x = 0.20	x = 0.25	x = 0.30	SnO ₂
A	222.758	225.651	232.401	234.330	237.223	237.223	238.187	246.866
В	272.903	271.938	274.831	274.831	274.831	274.831	275.796	_
C	285.439	285.439	287.368	286.403	286.403	287.368	287.368	289.296
D	326.905	322.083	324.976	324.012	324.012	319.190	324.012	311.476
E	369.335	369.335	371.264	371.264	372.228	371.264	372.228	_
F	459.981	459.981	_	_	_	_	_	_
G	467.696	_	_	_	472.517	_	475.410	_
Н	476.374	476.374	475.410	475.410	476.374	481.196	478.303	482.160
I	513.983	_	_	_	_	_	_	_
J	522.662	522.662	_	_	_	_	594.986	616.201
K	621.023	623.916	626.808	628.737	625.844	629.701	629.701	644.166
L	692.382	692.382	695.275	695.275	694.311	691.418	691.418	_
M	_	_	736.741	735.777	734.812	735.777	735.777	_
N	-	_	_	_	_	_	774.350	_

The FTIR data of pure Ga₂O₃ and SnO₂ are also presented for comparison

small fluctuation on position with no apparent trend but narrows as the Sn concentration increased.

increasing Sn concentration. Specifically, the trend noted for peaks A, C, H, and K is presented. These



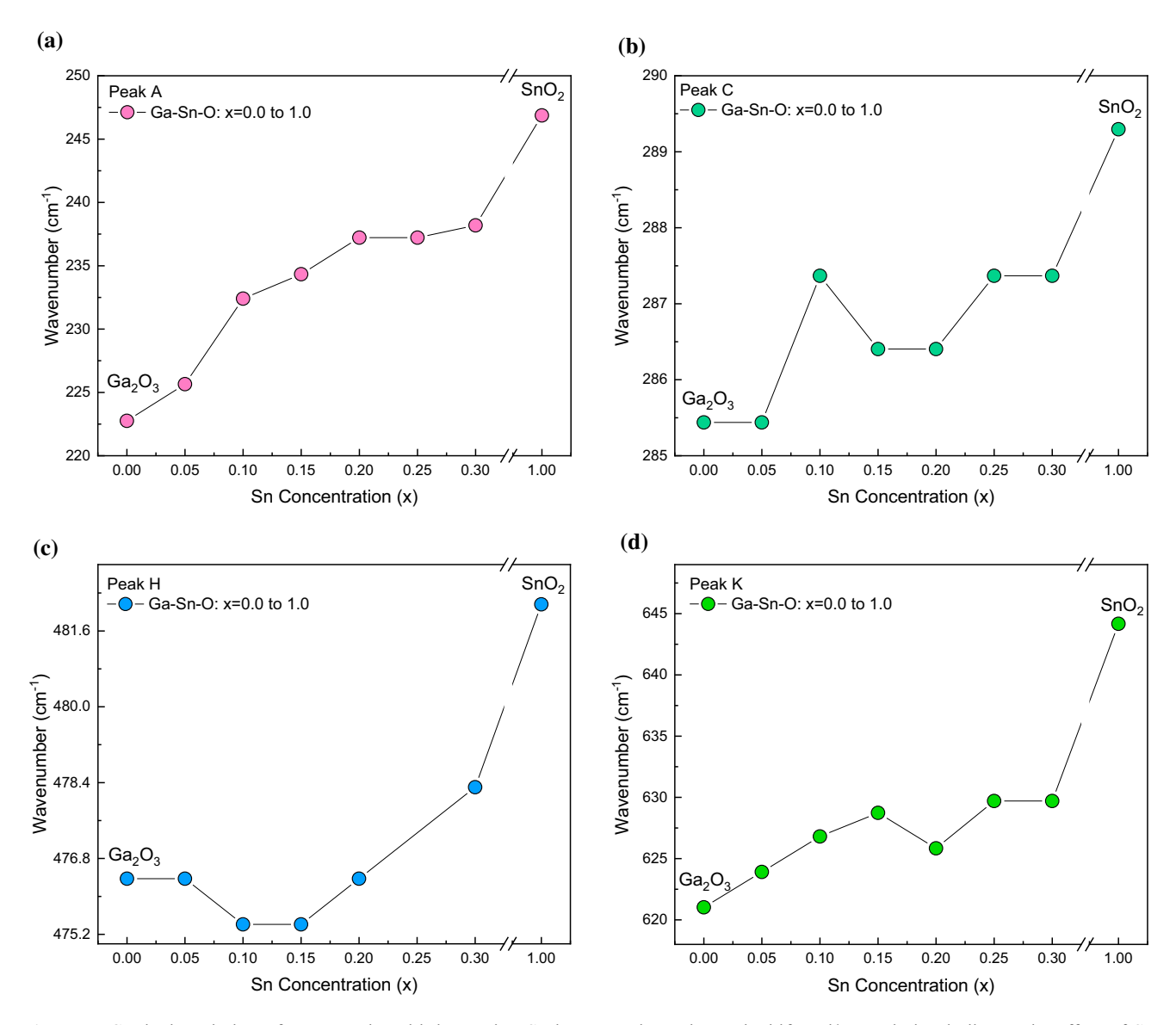


Figure 7 Gradual evolution of FTIR peaks with increasing Sn incorporation. The peak shift and/or evolution indicates the effect of Sn incorporation on the chemical bonding in Ga–Sn–O samples.

peaks were chosen due to proximity of Ga_2O_3 - and SnO_2 -related FTIR peaks. Gradual modulation of such spectroscopic signature has ability to understand the nature of atomic interaction while understanding the chemical bonding evolution in the complex Ga-Sn-O composite. Throughout the IR spectral region, SnO_2 corresponding signature peaks were at the higher value than that of Ga_2O_3 . As we increased the concentration of Sn in the composite structure, there was a chronological increment of peak positions. We believe such typical behavior was due to substitutional/interstitial alloying of Sn into Ga_2O_3 matrix. Assertively there was a significant modulation of IR transmission signature toward

SnO₂ as we increased the percentage of alloying. Additionally, few characteristic Ga₂O₃ peaks, F, G, I, and J, gradually disappeared with increasing Sn incorporation. M and N peaks were not assigned to neither Ga₂O₃ nor SnO₂ but were present on Sndoped samples. Dominance of Ga–Sn–O than its binary form (Ga₂O₃ and SnO₂) was responsible for this typical behavior. Compiling structural, optical, topographical, and IR active lattice vibrational characteristics; altogether, it was conclusive that during formation of complex ternary Ga–Sn–O compound with increasing amount of Sn there was an acute competition between substitutional and interstitial replacement of Ga atoms and parallel SnO₂ phase



formation inside the host material. For lower values of Sn alloying, there was a perfect formation of anticipated Ga–Sn–O compound. Increasing percentage of Sn beyond solubility limit promoted an isolated pure SnO₂ phase formation and introduced chemical inhomogeneity.

Electronic structure and chemical valence states

The XPS survey spectra (not shown) indicated the presence of all the expected elements i.e., Ga, Sn, and O, while the carbon (C 1 s) signal was also present in all survey spectra. The presence of C 1 s was due to the adventitious carbon adsorbed on sample surface due to exposure in air before they were introduced into XPS system. The core-level photoelectron spectra of the Ga 2p doublet, as observed in Ga-Sn-O samples, are shown in Fig. 8. The shape and BE values for the Ga $2p_{3/2}$ and Ga $2p_{1/2}$ peaks represented explicitly to those in stoichiometric Ga₂O₃. Note that the BE of Ga 2p doublet peaks (i.e., Ga $2p_{3/2}$ and Ga $2p_{1/2}$) for metallic Ga is: 1117.0 and 1144.0 eV, respectively [13, 32, 34, 35, 37, 61]. Therefore, the higher BE values of Ga 2p_{3/2} and Ga 2p_{1/2} peaks characterize the highest chemical valence state of Ga ions (Ga³⁺) in all the Ga-Sn-O samples. Though, Ga 3d high-resolution peaks were also collected, but the Ga 2p region was chosen over the Ga 3d region for analysis to avoid the interference of the Ga 3d peak with the O 2 s peak [7, 10]. The chemical shifts observed for both the Ga 2p and Ga 3d peaks were quite similar. Thus, analyses of the Ga 2p core level XPS can provide information about the nature of the Ga-O chemical bonding and Ga valence state in the Ga-Sn-O compounds. As shown in Fig. 8, no shift in the peak position is noted. Also, no variation in full-width at half-maximum (FWHM) was observed for these Ga peaks. Therefore, based on the XPS data, the chemical valence state of Ga ions was not affected by the Snincorporation into Ga₂O₃.

The complex chemistry of Ga–Sn–O compounds, especially the Sn-incorporation chemistry, was further examined by considering the Sn core level XPS peaks (Fig. 9). The XPS peaks related to Sn are Sn 3p and Sn 3d. The Sn 3p peak (Fig. 9a) showed a gradual increase in peak intensity with increasing x values indicating the fact that the Sn content increased in the samples. As widely used and accepted in the literature, the chemical valence states and chemistry of Sn

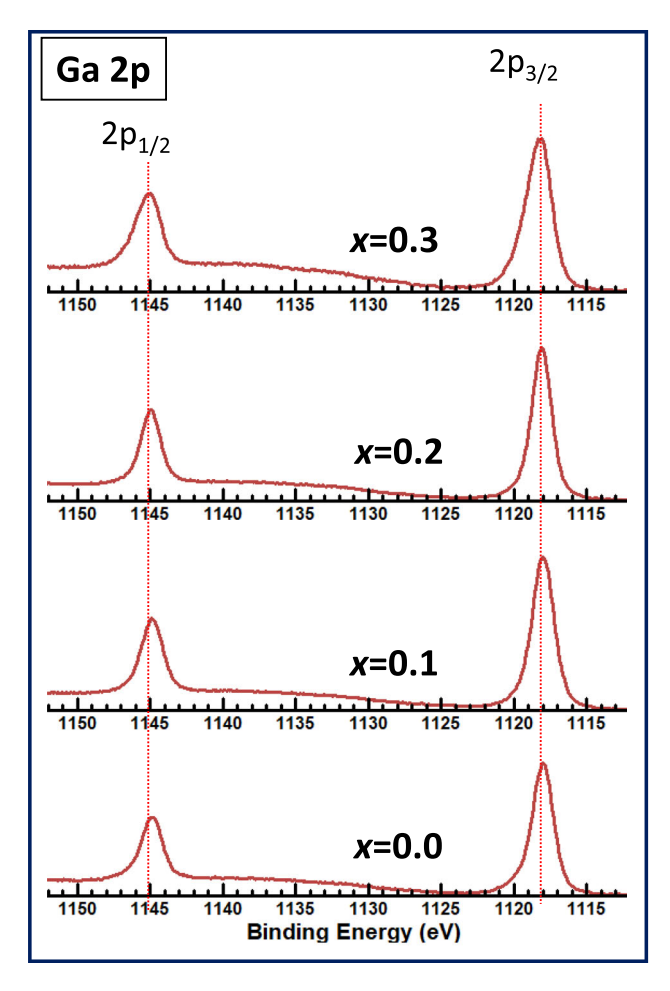
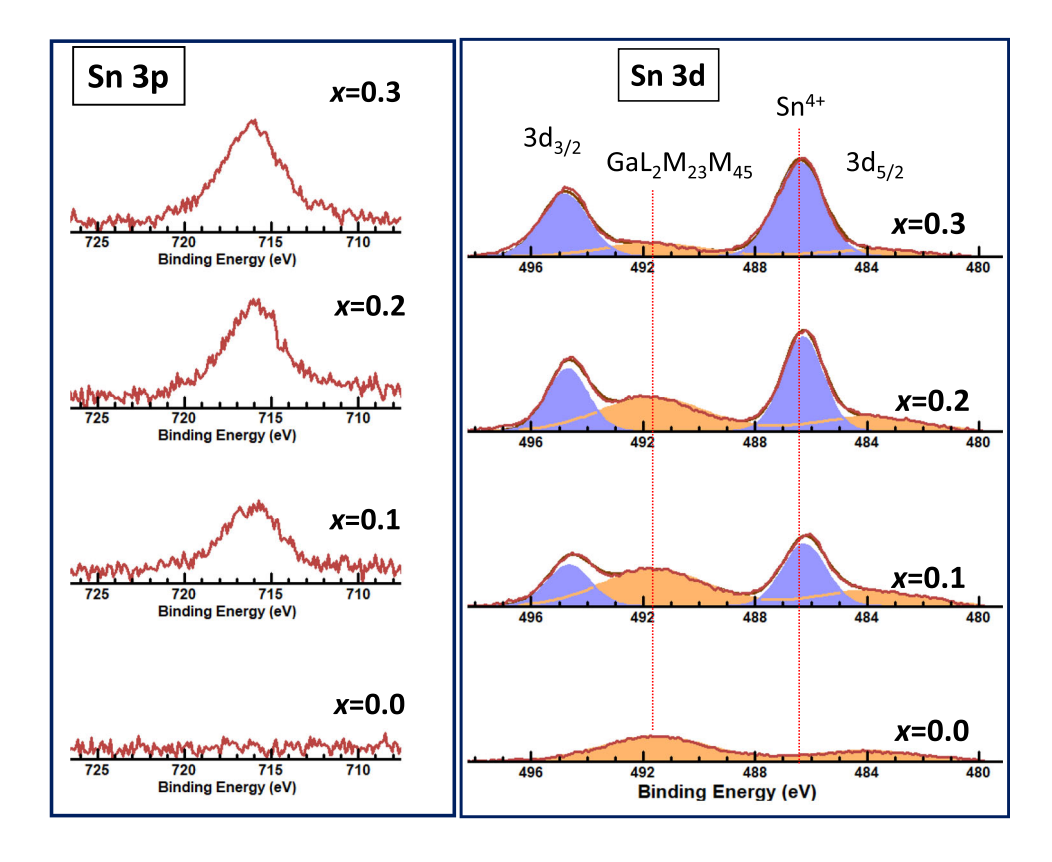


Figure 8 Ga 2p core-level XPS data of Ga–Sn–O samples. The Ga 2p peak positions and data confirm the existence of Ga in its highest oxidation state in all of the samples. No change in BE or peak shape is seen with Sn content into Ga–Sn–O samples. Therefore, Sn-incorporation didn't affect the chemical valence states of Ga ions in all of the samples.

doping/alloying can be revealed by means of Sn 3d peaks and their evolution. Under varying composition, the Sn 3d peaks are shown in Fig. 8b for Ga–Sn–O samples. It is evident that the Sn 3d peak exhibits a doublet, which corresponds to Sn 3d_{3/2} and Sn 3d_{5/2}, respectively. The BE values of these components are located at 494 and 486 eV, respectively, characterizing Sn ions in their highest chemical valence state (Sn⁴⁺) [72, 73]. Note that the Sn-oxide chemistry is very complex due to the fact that the Sn–O system contains various oxides, namely SnO₂, Sn₂O₃, Sn₃O₄, Sn₅O₆, and SnO, with variable chemical valence states [51, 74, 75]. However, only SnO₂ (Sn⁴⁺) and SnO (Sn²⁺) are thermodynamically stable. In fact, formation of these two oxide components is reported for



Figure 9 Sn core level 3p (a) and duplet 3d (b) spectra, extracted from Ga–Sn–O samples with increasing doping concentration. Gradual increment of both the peaks along with Sn incorporation supports the doping pattern.



Sn-doping into Ga₂O₃ nanomaterials, although the extent and SnO/SnO2 ratio depends on the conditions employed for synthesis. In the present case of Ga-Sn-O samples synthesized by the high-temperature solid-state reaction, it resulted into absence of such lower valence chemical states. Perhaps, the high-temperature process employed for sample preparation could be the reason for existence of Sn⁴⁺ in all Ga-Sn-O samples. The area of the Sn⁴⁺ spectra was larger than that of the Sn²⁺ spectra for all Sn concentration in Ga-Sn-O compound, indicating that the formation of SnO₂ was preferred to SnO due to the lower Gibbs free energy of formation of SnO₂ compared to that of SnO [32]. As the Sn concentration increased further, the Sn²⁺/Sn⁴⁺ area ratio continued to increase, indicating that the formation of SnO was also favorable at the higher Sn concentration, as shown in Fig. 9b.

The O 1 s spectra of Ga–Sn–O samples (Fig. 10) show that oxygen can be presented in various chemical states such as SnO, SnO₂, Ga₂O₃, and hydroxyl groups (OH–). Starting with pure β -Ga₂O₃, O 1 s peak has been shown for all Ga–Sn–O alloy. Asymmetric behavior of the O1s peak was deconvoluted into three different peaks, namely O–C, O–H and O–Ga. Undoubtedly, the O–Ga peak around

531 eV is the dominant among all. This also confirms the host matrix with highest Ga valence state, as reported in the literature [34, 37]. The shoulder peaks at 532 and 533 eV are indicating partially contaminated bare substrate of the composite host with carbon and water vapor. This kind of contamination related O 1 s peak is well documented in the literature and almost unavoidable. But we believe the bulk material is immune to these and can be fund through XPS analysis after in-situ etching of the top surface. Also, the relative intensity of O-C and O-H in comparison with O-Ga increased drastically for x = 0.3. Conclusion from previous section indicates that Sn incorporation beyond its solubility limit resulted in chemical inhomogeneity and phase segregation of SnO₂ from the host matrix through drastic rupture of the dominant Ga-Sn-O grain and formed disintegrated broken particles with excessive amount of broken bonds. This might be the reason behind greater formation of O-C and O-H bonds and successive dominance of corresponding O1s peaks.

The valence band (VB) XPS spectra of Ga–Sn–O samples are shown in Fig. 11. The data shown are for samples with variable Sn-concentration. Note that the analysis of VB XPS data can provide information on the valence band maximum (VBM), the density of



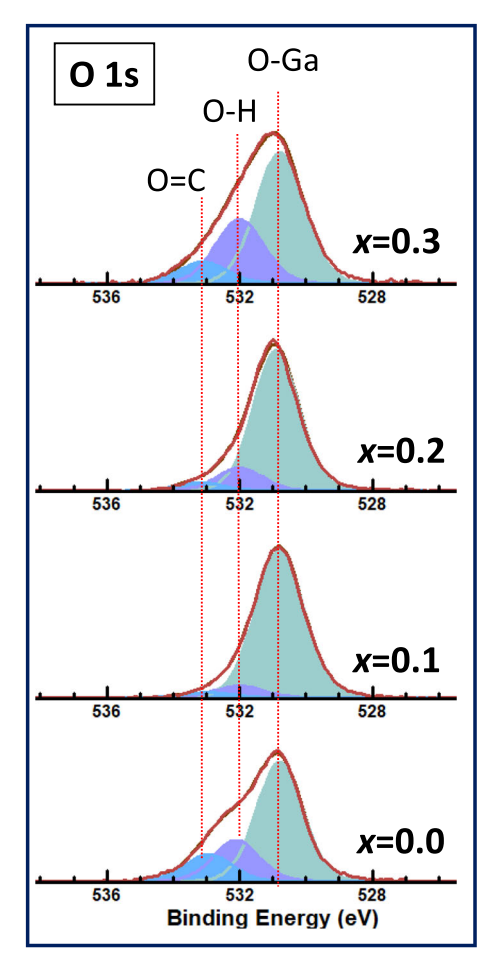


Figure 10 O 1 s core-level XPS patterns of Ga–Sn–O samples with increasing doping concentration.

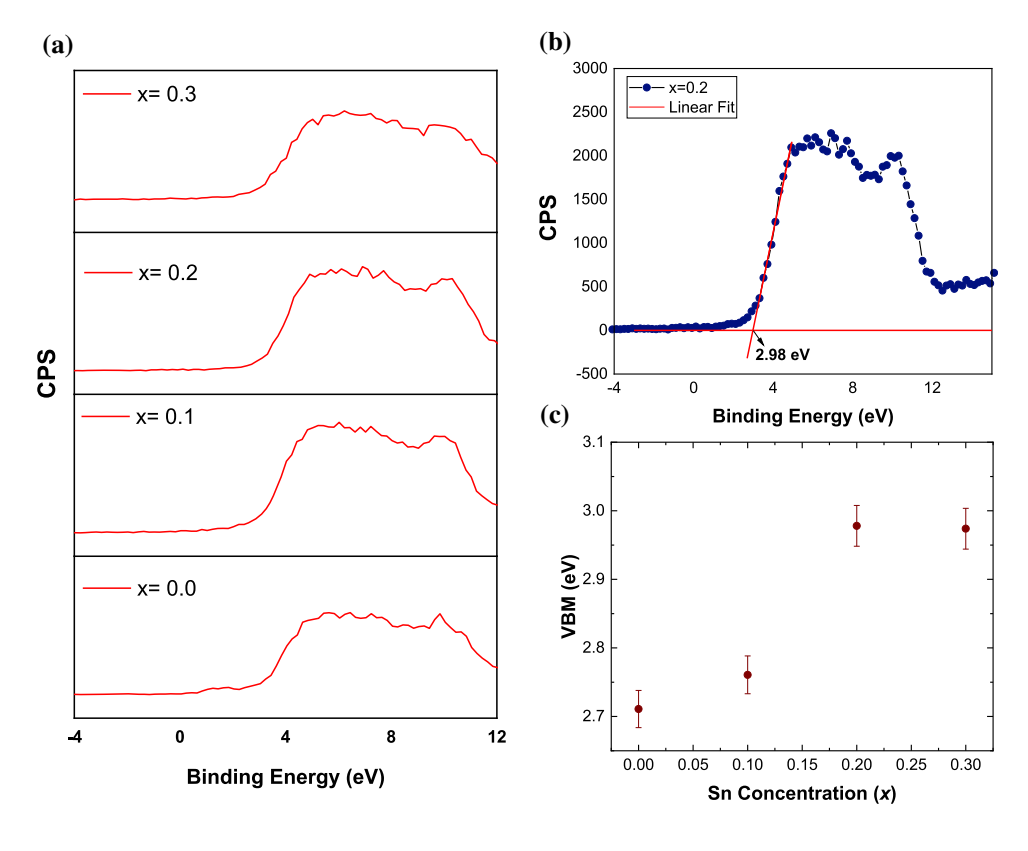
states (DOS), and Fermi-level position relative to VBM. In the present case, extrapolation of the leading edge to background line (zero counts) provided the VBM while the BE corresponding to 0 eV represents the Fermi-level position relative to the VBM. The VBM measured for intrinsic Ga₂O₃ polycrystalline samples is ~ 2.72 eV, which is in reasonably good agreement with those values (2.4-3.2 eV) reported in the literature. However, the VBM is sensitive to growth conditions, microstructure, defects, and thin films versus bulk or single crystals, and also the strain involved (for hetero-structured epilayers). In this case, with increasing Sn concentration, the VBM increased to 2.98 eV. The variation in VBM with Snconcentration is shown in Fig. 11c. Although VBM shift was slow at the initial concentration, the shift noted was significant at higher Sn concentration (x = 0.2-0.3). Also, the VBM for x = 0.30 reduced slightly than that of x = 0.20.

This overall tailoring of VBM in Ga-Sn-O composites, prepared through high temperature sintering, can be explained by means of relative modulation of single-phase versus multiphase complex Ga-Sn-O composite. It is well known that SnO₂ has red shifted optical band gap in comparison with Ga₂O₃ and carries relatively higher value of VBM. Assertively, Ga-Sn-O composite with increasing amount of Sn incorporation should show a progressive nature of VBM. Such as overall composite is going through a transformation from pure Ga2-O₃_SnO₂. But, this typical behavior is sustainable if the Sn concentration is within the solubility limit. Beyond this critical Sn concentration, it showed chemical inhomogeneity along with coexistence of multiphase composites. Previously we have shown that such higher concentration resulted into fragmented Ga-Sn-O + SnO₂ complex composite with drastic change in morphological behavior. Also, the Sn concentration into Ga-Sn-O matrix remained constant after this critical point and excess Sn segregated as binary SnO₂ form. The saturation of VBM after x = 0.20 is reflecting the aforementioned stabilization of complex composites. There is existing literature, supporting such tailoring of Ga₂O₃ thin film or bulk VBM with external doping or alloying. Other metal oxide systems also follow similar behavior with foreign impurity.

Finally, we turn our attention not to explain the implications of chemical inhomogeneity and changes in the chemical bonding as a function of Sn-doping on the electrical and optical properties of the Ga-Sn-O materials. As is well known, changes in the chemical bond due to foreign atoms and/or composite phases induce changes in the dielectric and optical properties of wide band gap semiconductors [76, 77]. Therefore, we expect that the Ga-Sn-O materials with variable Sn concentration may offer means to derive tunable dielectric properties. In fact, the optical properties of Ga-Sn-O materials are seen to be variable as a function of Sn-content, as reported elsewhere³. Specifically, the optical absorption in these Ga-Sn-O materials was fully dependent on the Sn concentration and associated changes. The band gap reduction with Sn-concentration was noted³. Specifically, for higher Sn content (*x*), the evolution of two absorption bands related to composite was evident³. The future efforts will be directed to evaluate the dielectric properties of Ga-Sn-O materials.



Figure 11 a Valence band (VB) XPS spectra of Ga–Sn–O samples, **b** calculation of valance band maxima. **c** Variation in VBM with increasing Sn concentration.



Conclusions

We have performed a detailed study on the structure, morphology, physical properties, chemical bonding, and electronic properties of Ga-Sn-O materials with varying Sn concentration. Probing the as prepared samples using different analytical methods revealed the modulation of phase and chemical inhomogeneity. High-temperature solid-state reaction-assisted chemical rearrangement of this complex metal oxide showed drastic transition of coexisting stable phases as the Sn concentration crossed the solubility limit. Starting with pure Ga₂O₃, initial Sn incorporation, below the solubility limit, settled in pure Ga-Sn-O composite. Particle size stayed comparable with the host material. Lattice vibration and electronic structure followed gradual evolution from binary Ga₂O₃ to ternary Ga-Sn-O compound. But, after the critical Sn concentration, beyond 15% as confirmed from structural characterization, excess Sn tried to segregate from the host matrix and introduced chemical inhomogeneity throughout the composite. As a result, grains of the host material became fragmented and showed increasing signature of segregated SnO₂ phase. Lattice vibration and electronic band alignment tailored accordingly. These results may be useful to optimize the Ga–Sn–O materials with tailored properties as desired for specific functionality in a given application.

Acknowledgements

The authors also acknowledge, with pleasure, support from the National Science Foundation (NSF) with NSF-PREM Grant #DMR-1827745. The authors express their sincere thanks for Ms. Rebecca Romero for her assistance with SEM and EDS measurements. This material is also based upon work supported by the Air Force Office of Scientific Research (AFOSR) under award number FA9550-21-1-0360. However, any opinions, findings, and conclusions or recommendations expressed in this material are those of the author(s) and do not necessarily reflect the views of the United States Air Force. A portion of the research (XPS measurements) was performed using Environmental Molecular Sciences Laboratory (EMSL), a national scientific user facility sponsored by the Department of Energy's Office of Biological and Environmental Research and located at Pacific Northwest National Laboratory.



Funding

This study was funded by the National Science Foundation (NSF) with NSF-PREM Grant #DMR-1827745.

Data availability

The scientific data and analyses are included in the manuscript. The other data that do not appear in the manuscript may be available by a reasonable request from the corresponding author.

Declarations

Conflict of interest The authors declare that they have no conflict of interest.

References

- [1] Castro-Fernández P, Blanco MV, Verel R, Willinger E, Fedorov A, Abdala PM, Müller CR (2020) Atomic-scale insight into the structure of metastable γ-Ga₂O₃ nanocrystals and their thermally-driven transformation to β-Ga₂O₃. J Phys Chem C 124(37):20578–20588
- [2] Uddin A, Bhuiyan AFM, Feng Z, Johnson JM, Huang H-L, Hwang J, Zhao H (2020) MOCVD epitaxy of ultrawide bandgap β-(Al_xGa_{1-x})₂O₃ with high-Al composition on (100) β-Ga₂O₃ substrates. Cryst Growth Des 20(10):6722–6730
- [3] Gutierrez G, Sundin EM, Nalam PG, Zade V, Romero R, Nair AN, Sreenivasan S, Das D, Li C, Ramana CV (2021) Interfacial phase modulation-induced structural distortion, band gap reduction, and nonlinear optical activity in tinincorporated Ga₂O₃. J Phys Chem C 125(37):20468–20481
- [4] Farvid SS, Wang T, Radovanovic PV (2011) Colloidal gallium indium oxide nanocrystals: a multifunctional lightemitting phosphor broadly tunable by alloy composition. J Am Chem Soc 133(17):6711–6719
- [5] Kim J, Mastro MA, Tadjer MJ, Kim J (2018) Heterostructure WSe₂-Ga₂O₃ junction field-effect transistor for low-dimensional high-power electronics. ACS Appl Mater Interfaces 10(35):29724–29729
- [6] Li KH, Alfaraj N, Kang CH, Braic L, Hedhili MN, Guo Z, Ng TK, Ooi BS (2019) Deep-ultraviolet photodetection using single-crystalline beta-Ga₂O₃/NiO heterojunctions. ACS Appl Mater Interfaces 11(38):35095–35104

- [7] Liang H, Cui S, Su R, Guan P, He Y, Yang L, Chen L, Zhang Y, Mei Z, Du X (2018) Flexible X-ray detectors based on amorphous Ga₂O₃ thin films. ACS Photonics 6(2):351–359
- [8] Nagarajan L, De Souza RA, Samuelis D, Valov I, Borger A, Janek J, Becker KD, Schmidt PC, Martin M (2008) A chemically driven insulator-metal transition in non-stoichiometric and amorphous gallium oxide. Nat Mater 7(5):391–398
- [9] Makeswaran N, Das D, Zade V, Gaurav P, Shutthanandan V, Tan S, Ramana CV (2021) Size-and phase-controlled nanometer-thick β-Ga₂O₃ films with green photoluminescence for optoelectronic applications. ACS Appl Nano Mater 4(4):3331–3338
- [10] Pratiyush AS, Krishnamoorthy S, Kumar S, Xia Z, Muralidharan R, Rajan S, Nath DN (2018) Demonstration of zero bias responsivity in MBE grown β-Ga₂O₃ lateral deep-UV photodetector. Jpn J Appl Phys 57(6):060313
- [11] Qiao B, Zhang Z, Xie X, Li B, Li K, Chen X, Zhao H, Liu K, Liu L, Shen D (2019) Avalanche gain in metal–semiconductor–metal Ga₂O₃ solar-blind photodiodes. J Phys Chem C 123(30):18516–18520
- [12] Park S, Yoon HJ (2018) New approach for large-area thermoelectric junctions with a liquid eutectic gallium-indium electrode. Nano Lett 18(12):7715–7718
- [13] Roy S, Mallesham B, Zade VB, Martinez A, Shutthanandan V, Thevuthasan S, Ramana CV (2018) Correlation between structure, chemistry, and dielectric properties of iron-doped gallium oxide (Ga_{2-x}Fe_xO₃). J Phys Chem C 122(48):27597–27607
- [14] Simeone FC, Yoon HJ, Thuo MM, Barber JR, Smith B, Whitesides GM (2013) Defining the value of injection current and effective electrical contact area for EGaIn-based molecular tunneling junctions. J Am Chem Soc 135(48):18131–18144
- [15] Su J, Guo R, Lin Z, Zhang S, Zhang J, Chang J, Hao Y (2018) Unusual Electronic and optical properties of twodimensional Ga₂O₃ predicted by density functional theory. J Phys Chem C 122(43):24592–24599
- [16] Higashiwaki M, Sasaki K, Murakami H, Kumagai Y, Koukitu A, Kuramata A, Masui T, Yamakoshi S (2016) Recent progress in Ga₂O₃ power devices. Semicond Sci Technol 31(3):034001
- [17] Higashiwaki M, Sasaki K, Kuramata A, Masui T, Yamakoshi S (2012) Gallium oxide (Ga₂O₃) metal-semiconductor field-effect transistors on single-crystal β-Ga₂O₃ (010) substrates. Appl Phys Lett 100(1):013504
- [18] Pearton SJ, Yang J, Cary PH, Ren F, Kim J, Tadjer MJ, Mastro MA (2018) A review of Ga₂O₃ materials, processing, and devices. Appl Phys Rev 5(1):011301



- [19] Geller S (1960) Crystal structure of β -Ga₂O₃. J Chem Phys 33(3):676–684
- [20] Víllora EG, Shimamura K, Yoshikawa Y, Ujiie T, Aoki K (2008) Electrical conductivity and carrier concentration control in β-Ga₂O₃ by Si doping. Appl Phys Lett 92(20):202120
- [21] Zhang F, Arita M, Wang X, Chen Z, Saito K, Tanaka T, Nishio M, Motooka T, Guo Q (2016) Toward controlling the carrier density of Si doped Ga₂O₃ films by pulsed laser deposition. Appl Phys Lett 109(10):102105
- [22] Leedy KD, Chabak KD, Vasilyev V, Look DC, Mahalingam K, Brown JL, Green AJ, Bowers CT, Crespo A, Thomson DB, Jessen GH (2018) Si content variation and influence of deposition atmosphere in homoepitaxial Si-doped β-Ga₂O₃ films by pulsed laser deposition. APL Mater 6(10):101102
- [23] Varley JB, Weber JR, Janotti A, Van de Walle CG (2010) Oxygen vacancies and donor impurities in β -Ga2O3. Appl Phys Lett 97(14):142106
- [24] Peelaers H, Van de Walle CG (2016) Doping of Ga₂O₃ with transition metals. Phys Rev B 94(19):195203
- [25] Peelaers H, Lyons JL, Varley JB, Van de Walle CG (2019) Deep acceptors and their diffusion in Ga₂O₃. APL Mater 7(2):022519
- [26] Tatsumi H, Teramura K, Huang Z, Wang Z, Asakura H, Hosokawa S, Tanaka T (2017) Enhancement of CO evolution by modification of Ga₂O₃ with rare-earth elements for the photocatalytic conversion of CO₂ by H₂O. Langmuir 33(49):13929–13935
- [27] Syed N, Zavabeti A, Mohiuddin M, Zhang B, Wang Y, Datta RS, Atkin P, Carey BJ, Tan C, van Embden J, Chesman ASR, Ou JZ, Daeneke T, Kalantar-zadeh K (2017) Sonication-assisted synthesis of gallium oxide suspensions featuring trap state absorption: test of photochemistry. Adv Funct Mater 27(43):1702295
- [28] Wang X, Shen S, Jin S, Yang J, Li M, Wang X, Han H, Li C (2013) Effects of Zn²⁺ and Pb²⁺ dopants on the activity of Ga₂O₃-based photocatalysts for water splitting. Phys Chem Chem Phys 15(44):19380–19386
- [29] Zhang W, Naidu BS, Ou JZ, O'Mullane AP, Chrimes AF, Carey BJ, Wang Y, Tang SY, Sivan V, Mitchell A, Bhargava SK, Kalantar-Zadeh K (2015) Liquid metal/metal oxide frameworks with incorporated Ga₂O₃ for photocatalysis. ACS Appl Mater Interfaces 7(3):1943–1948
- [30] Tien L-C, Chen W-T, Ho C-H (2011) Enhanced Photocatalytic activity in β -Ga₂O₃ nanobelts. J Am Ceram Soc 94(9):3117–3122
- [31] Layek A, Yildirim B, Ghodsi V, Hutfluss LN, Hegde M, Wang T, Radovanovic PV (2015) Dual europium luminescence centers in colloidal Ga₂O₃ nanocrystals: controlled

- in situ reduction of Eu(III) and stabilization of Eu(II). Chem Mater 27(17):6030–6037
- [32] Bandi M, Zade V, Roy S, Nair AN, Seacat S, Sreenivasan S, Shutthanandan V, Van de Walle CG, Peelaers H, Ramana CV (2020) Effect of titanium induced chemical inhomogeneity on crystal structure, electronic structure, and optical properties of wide band gap Ga₂O₃. Cryst Growth Des 20(3):1422–1433
- [33] Dakhel AA (2011) Structural, optical, and opto-dielectric properties of W-doped Ga₂O₃ thin films. J Mater Sci 47(7):3034–3039
- [34] Roy S, Ramana CV (2021) Effect of sintering temperature on the chemical bonding, electronic structure and electrical transport properties of β-Ga_{1.9}Fe0.1O3 compounds. J Mater Sci Technol 67:135–144
- [35] Mallesham B, Roy S, Bose S, Nair AN, Sreenivasan S, Shutthanandan V, Ramana CV (2020) Crystal chemistry, band-gap red shift, and electrocatalytic activity of iron-doped gallium oxide ceramics. ACS Omega 5(1):104–112
- [36] Zade V, Mallesham B, Shantha-Kumar S, Bronson A, Ramana CV (2019) Interplay between solubility limit, structure, and optical properties of tungsten-doped Ga₂O₃ compounds synthesized by a two-step calcination process. Inorg Chem 58(6):3707–3716
- [37] Rubio EJ, Mates TE, Manandhar S, Nandasiri M, Shutthanandan V, Ramana CV (2016) tungsten incorporation into gallium oxide: crystal structure, surface and interface chemistry, thermal stability, and interdiffusion. J Phys Chem C 120(47):26720–26735
- [38] Zhang Y, Yan J, Li Q, Qu C, Zhang L, Xie W (2011) Optical and structural properties of Cu-doped β-Ga₂O₃ films. Mater Sci Eng, B 176(11):846–849
- [39] Chen C-C, Chen C-C (2011) Morphology and electrical properties of pure and ti-doped gas-sensitive Ga₂O₃ film prepared by rheotaxial growth and thermal oxidation. J Mater Res 19(4):1105–1117
- [40] Rubio EJ, Ramana CV (2013) Tungsten-incorporation induced red-shift in the bandgap of gallium oxide thin films. Appl Phys Lett 102(19):191913
- [41] Oleksak RP, Stickle WF, Herman GS (2015) Aqueous-based synthesis of gallium tungsten oxide thin film dielectrics. J Mater Chem C 3(13):3114–3120
- [42] Archer PI, Radovanovic PV, Heald SM, Gamelin DR (2005) Low-temperature activation and deactivation of high-curietemperature ferromagnetism in a new diluted magnetic semiconductor: Ni²⁺-doped SnO₂. JACS 127(41):14479–14487
- [43] Aguir K, Bernardini S, Lawson B, Fiorido T (2020) Trends in metal oxide thin films: Synthesis and applications of tin oxide. In: *Tin oxide materials*, pp 219–246



- [44] Batzill M, Diebold U (2005) The surface and materials science of tin oxide. Prog Surf Sci 79(2-4):47-154
- [45] Das S, Jayaraman V (2014) SnO₂: a comprehensive review on structures and gas sensors. Prog Mater Sci 66:112–255
- [46] Chen M, Zhang C, Li L, Liu Y, Li X, Xu X, Xia F, Wang W, Gao J (2013) Sn powder as reducing agents and SnO₂ precursors for the synthesis of SnO₂-reduced graphene oxide hybrid nanoparticles. ACS Appl Mater Interfaces 5(24):13333–13339
- [47] Kim HW, Na HG, Kwon YJ, Kang SY, Choi MS, Bang JH, Wu P, Kim SS (2017) Microwave-assisted synthesis of graphene-SnO₂ nanocomposites and their applications in gas sensors. ACS Appl Mater Interfaces 9(37):31667–31682
- [48] Xu X, Zhuang J, Wang X (2008) SnO₂ quantum dots and quantum wires: controllable synthesis, self-assembled 2D architectures, and gas-sensing properties. JACS 130(37):12527–12535
- [49] Savioli J, Gavin AL, Lucid AK, Watson GW (2020) The structure and electronic structure of tin oxides. In: *Tin oxide* materials, pp 11–39
- [50] Zhang J, Xia C, Deng Q, Xu W, Shi H, Wu F, Xu J (2006) Growth and characterization of new transparent conductive oxides single crystals β-Ga₂O₃: Sn. J Phys Chem Solids 67(8):1656–1659
- [51] Ryou H, Yoo TH, Yoon Y, Lee IG, Shin M, Cho J, Cho BJ, Hwang WS (2020) Hydrothermal synthesis and photocatalytic property of Sn-doped β-Ga₂O₃ nanostructure. ECS J Solid State Sci Technol 9(4):045009
- [52] Orita M, Ohta H, Hirano M, Hosono H (2000) Deep-ultraviolet transparent conductive β -Ga₂O₃ thin films. Appl Phys Lett 77(25):4166–4168
- [53] Guo D, Su Y, Shi H, Li P, Zhao N, Ye J, Wang S, Liu A, Chen Z, Li C, Tang W (2018) Self-powered ultraviolet photodetector with superhigh photoresponsivity (3.05 A/W) based on the GaN/Sn:Ga₂O₃ pn junction. ACS Nano 12(12):12827–12835
- [54] Knight S, Mock A, Korlacki R, Darakchieva V, Monemar B, Kumagai Y, Goto K, Higashiwaki M, Schubert M (2018) Electron effective mass in Sn-doped monoclinic single crystal β-gallium oxide determined by mid-infrared optical Hall effect. Appl Phys Lett 112(1):012103
- [55] Dang GT, Kawaharamura T, Furuta M, Allen MW (2015) Mist-CVD grown Sn-doped α-Ga₂O₃ MESFETs. IEEE Trans Electron Devices 62(11):3640–3644
- [56] Zhao JL, Sun XW, Ryu H, Tan ST (2011) UV and visible electroluminescence from a Sn:Ga₂O₃/n+-Si heterojunction by metal-organic chemical vapor deposition. IEEE Trans Electron Devices 58(5):1447–1451
- [57] Hao SJ, Hetzl M, Schuster F, Danielewicz K, Bergmaier A, Dollinger G, Sai QL, Xia CT, Hoffmann T, Wiesinger M,

- Matich S, Aigner W, Stutzmann M (2019) Growth and characterization of β -Ga₂O₃ thin films on different substrates. J ApplPhys 125(10):105701
- [58] Ohira S, Suzuki N, Arai N, Tanaka M, Sugawara T, Nakajima K, Shishido T (2008) Characterization of transparent and conducting Sn-doped β-Ga₂O₃ single crystal after annealing. Thin Solid Films 516(17):5763–5767
- [59] Kawaharamura T, Dang GT, Furuta M (2012) Successful growth of conductive highly crystalline Sn-Doped α-Ga₂O₃ thin films by fine-channel mist chemical vapor deposition. Jpn J Appl Phys 51:040207
- [60] Ristić M, Popović S, Musić A (2005) Application of sol-gel method in the synthesis of gallium (III)-oxide. Mater Lett 59(10):1227–1233
- [61] Ramana CV, Roy S, Zade V, Battu AK, Makeswaran N, Shutthanandan V (2021) Electronic structure and chemical bonding in transition-metal-mixed gallium oxide (Ga₂O₃) compounds. J Phys Chem Solids 157:110174
- [62] Rambabu U, Munirathnam NR, Prakash TL, Vengalrao B, Buddhudu S (2007) Synthesis and characterization of morphologically different high purity gallium oxide nanopowders. J Mater Sci 42(22):9262–9266
- [63] Cheng Y, Chen J, Yang K, Wang Y, Yin Y, Liang H, Du G (2014) Structural, morphological, FTIR and photoluminescence properties of gallium oxide thin films. J Vac Sci Technol B 32(3):03D119
- [64] Sun C, Deng J, Kong L, Chen L, Shen Z, Cao Y, Zhang H, Wang X (2017) Structure and photoluminescence properties of β-Ga₂O₃ nanofibres synthesized via electrospinning method. IOP Conf Ser: Mater Sci Eng 275:012046
- [65] Quan Y, Fang D, Zhang X, Liu S, Huang K (2010) Synthesis and characterization of gallium oxide nanowires via a hydrothermal method. Mater Chem Phys 121(1):142–146
- [66] Ganguly BN, Verma V, Chatterjee D, Satpati B, Debnath S, Saha P (2016) Study of gallium oxide nanoparticles conjugated with β-cyclodextrin: an application to combat cancer. ACS Appl Mater Interfaces 8(27):17127–17137
- [67] Song KC, Kang Y (2000) Preparation of high surface area tin oxide powders by a homogeneous precipitation method. Mater Lett 42(5):283–289
- [68] Abruzzi RC, Dedavid BA, Pires MJR (2015) Characterization of tin dioxide nanoparticles synthesized by oxidation. SciELO: Cerâmica [online] 61:328–333
- [69] Khanom R, Akter S, Ahmed S, Shahjahan M, Qadir MR (2017) Synthesis of SnO₂ nanopowders for advanced ceramics and electronic sensor transducer devices and characterization and band gap. Nanosci Nometrol 3:12–19
- [70] Farrukh MA, Heng BT, Adnan R (2010) Surfactant-controlled aqueous synthesis of SnO₂ nanoparticles via the



- hydrothermal and conventional heating methods. Turk J Chem 34:537-550
- [71] Marikkannan M, Vishnukanthan V, Vijayshankar A, Mayandi J, Pearce JM (2015) A novel synthesis of tin oxide thin films by the sol-gel process for optoelectronic applications. AIP Adv 5(2):027122
- [72] Jung EH, Chen B, Bertens K, Vafaie M, Teale S, Proppe A, Hou Y, Zhu T, Zheng C, Sargent EH (2020) Bifunctional surface engineering on SnO₂ reduces energy loss in perovskite solar cells. ACS Energy Lett 5(9):2796–2801
- [73] Kakinuma K, Suda K, Kobayashi R, Tano T, Arata C, Amemiya I, Watanabe S, Matsumoto M, Imai H, Iiyama A, Uchida M (2019) Electronic states and transport phenomena of Pt nanoparticle catalysts supported on Nb-doped SnO₂ for polymer electrolyte fuel cells. ACS Appl Mater Interfaces 11(38):34957–34963
- [74] Zeng W, Liu Y, Chen G, Zhan H, Mei J, Luo N, He Z, Tang C (2020) SnO–Sn₃O₄ heterostructural gas sensor with high

- response and selectivity to parts-per-billion-level NO₂ at low operating temperature. RSC Adv 10(50):29843–29854
- [75] Pan XQ, Fu L (2001) Oxidation and phase transitions of epitaxial tin oxide thin films on (1012) sapphire. J Appl Phys 89(11):6048–6055
- [76] Kalidindi NR, Manciu FS, Ramana CV (2011) Crystal structure, phase, and electrical conductivity of nanocrystalline W_{0.95}Ti_{0.05}O₃ thin films. ACS Appl Mater Interfaces 3:863–868
- [77] Lia Y-J, Gonga P, Li S-L, Lia Y-L, Ma W-D, Fang X-Y, Yang Y-Y, Cao M-S (2020) Effects of hydroxyl groups and hydrogen passivation on the structure, electrical and optical properties of silicon carbide nanowires. Phys Lett 384:126106

Publisher's Note Springer Nature remains neutral with regard to jurisdictional claims in published maps and institutional affiliations.

